Evaluation of Non-invasive Ankle Joint Effort Prediction Methods for Use in Neurorehabilitation Using Electromyography and Ultrasound Imaging

Qiang Zhang, Member, IEEE, Ashwin Iyer, Kang Kim*, and Nitin Sharma*, Member, IEEE

Abstract-Objective: Reliable measurement of voluntary human effort is essential for effective and safe interaction between the wearer and an assistive robot. Existing voluntary effort prediction methods that use surface electromyography (sEMG) are susceptible to prediction inaccuracies due to non-selectivity in measuring muscle responses. This technical challenge motivates an investigation into alternative non-invasive effort prediction methods that directly visualize the muscle response and improve effort prediction accuracy. The paper is a comparative study of ultrasound imaging (US)-derived neuromuscular signals and sEMG signals for their use in predicting isometric ankle dorsiflexion moment. Furthermore, the study evaluates the prediction accuracy of model-based and model-free voluntary effort prediction approaches that use these signals. Methods: The study evaluates sEMG signals and three US imaging-derived signals: pennation angle, muscle fascicle length, and echogenicity and three voluntary effort prediction methods: linear regression (LR), feedforward neural network (FFNN), and Hill-type neuromuscular model (HNM). Results: In all the prediction methods, pennation angle and fascicle length significantly improve the prediction accuracy of dorsiflexion moment, when compared to echogenicity. Also, compared to LR, both FFNN and HNM improve dorsiflexion moment prediction accuracy. Conclusion: The findings indicate FFNN or HNM approach and using pennation angle or fascicle length predict human ankle movement intent with higher accuracy. Significance: The accurate ankle effort prediction will pave the path to safe and reliable robotic assistance in patients with drop foot.

Index Terms—Ankle dorsiflexion, Ultrasound imaging, Electromyography, Linear regression, Feedforward neural network, Neuromuscular model

Manuscript received December 27, 2019; revised June 24, 2020; accepted July 27, 2020. Date of publication XXXX, 2020. This work was supported by the NSF CAREER under Award 1750748. (Corresponding authors: Kang Kim; Nitin Sharma.)

Q. Zhang, A. Iyer, and N. Sharma are with the UNC/NC State Joint Department of Biomedical Engineering, NC State University, Raleigh, NC 27695 USA (e-mail: qzhang25@ncsu.edu; aiyer3@ncsu.edu; nsharm23@ncsu.edu).

K. Kim is with the Department of Bioengineering, School of Engineering, University of Pittsburgh, Pittsburgh, PA 15260 USA, with the Center for Ultrasound Molecular Imaging and Therapeutics, Department of Medicine and Heart and Vascular Institute, University of Pittsburgh School of Medicine and University of Pittsburgh Medical Center, Pittsburgh, PA 15213 USA, with the Department of Mechanical Engineering and Materials Science, School of Engineering, University of Pittsburgh, PH 15260 USA, and also with the McGowan Institute for Regenerative Medicine, University of Pittsburgh and University of Pittsburgh Medical Center, Pittsburgh, PA 15219 USA (e-mail: kangkim@upmc.edu).

Copyright (c) 2020 IEEE. Personal use of this material is permitted. However, permission to use this material for any other purposes must be obtained from the IEEE by sending an email to pubs-permissions@ieee.org.

I. Introduction

Ankle dorsiflexion plays an essential role in activities of daily living (ADLs), like walking, sitting to standing, and balance control [1]. The weakened function or dysfunction of ankle dorsiflexion, like drop foot, impedes ankle movements. Powered ankle exoskeletons and functional electrical stimulation (FES) are potential neurorehabilitation technologies that can enable people with ankle weakness or dysfunction to regain the function [2], [3]. To facilitate motor relearning, these neurorehabilitation technologies use "assist-as-needed" control [4], [5]. This neurorehabilitation control strategy provides FES or robotic assistance based on a user's movement intent or voluntary effort, which can be determined by measuring any or combination of the following modalities: neural signals originating from the central nervous system, electrical activity of the muscles when neurally excited, muscle force, limb kinematics, and joint torques [6]. Both the efficacy of the neurorehabilitation and the safety of the user depends on accurately determining the user's voluntary effort or intent.

Existing intent detection or prediction approaches can be broadly categorized into mechanical and neuromuscular approaches. Mechanical approaches directly measure the physical human-machine-interaction (pHMI) through force or torque or limb kinematic measurements [7], [8]. However, there are two shortcomings in this approach. First, the installation of a mechanical sensor needs an exoskeletal frame, which limits the portability of the entire device. Second, interaction between a human limb and a robotic device is prone to misalignments between rotation centers of a human joint and an exoskeleton joint, which may induce undesired interaction force [9], [10].

Compared to the mechanical approaches, neuromuscular approaches predict voluntary effort by correlating neuromuscular signals with the joint moment or joint kinematics. Surface electromyography (sEMG) is a commonly used neuromuscular signal to measure voluntary skeletal muscle activity [11], [12]. However, sEMG is sensitive to measurement noise and signal cross-talk or interference from adjacent muscle groups. sEMG is also least useful in measuring a deeply-located muscle's activity. Ultrasound (US) imaging is an alternative sensing technique that can directly visualize targeted muscle activity at different depths with low signal interference. However, unlike sEMG, processing to obtain an image from US raw radio frequency (RF) data is time-consuming and difficult for real-

time implementation. Given the advantages and disadvantages of US imaging and sEMG, a motivation exists to examine, which one of these neuromuscular signals is more suitable for intent prediction. Further, it is unclear which voluntary prediction approach is the most effective mapping function between the sEMG or US imaging-derived surrogate signals and a limb joint force or movement.

We divide the determination of the mapping function into model-free and model-based categories. In model-free methods, a machine learning approximation builds a mathematical relationship between a neuromuscular signal such as sEMG or muscle structural or functional parameters derived from US images like pennation angle (PA), muscle fascicle length (FL), muscle thickness, and echogenicity and the measured human limb force or movement. These mathematical relationships use a combination of basis functions, e.g., linear or nonlinear polynomials [13], exponential or Gaussian functions [12], as well as linear or nonlinear regression [14], [15]. Sikdar et al. [16] analyzed real-time US images of the forearm muscles to classify the intent of finger movements. Activity maps, created using a nearest neighbor classifier, used changes in the US echogenicity of the forearm muscles. In their recent work [17], Pearson's correlation coefficient (PCC) was used between the rest frame and other US frames in the motion sequence to classify volitional motion intention. The objective was to predict intent during a virtual target grasp and a holding task for 5 different hand motions in a virtual environment. An artificial neural network (ANN) is another model-free approach that can be used to map the neuromuscular signals to voluntary effort [18], [19]. Savelberg et al. [18] adopted an ANN to predict dynamic tendon forces of the gastrocnemius muscles of three cats by measuring their EMG signals. However, very few contributions exist that use ANN-based human motion intent detection by using parameters extracted from US images.

The aforementioned model-free approaches are essentially black box approaches. The functional relationship between neuromuscular signals and mechanical functions are established without explicit equations. A Hill-type neuromuscular model (HNM) is most frequently used for establishing a cause-effect mapping between a neuromuscular signal and the joint moment. Lloyd et al. [11] proposed a generic EMG driven musculoskeletal model to predict inverse dynamic joint moments. The model parameters were calibrated by using a nonlinear least-squares approach, sEMG-based estimation of neuromuscular excitation has also been utilized to drive HNM during a wide range of human dynamic motor functionalities, like muscle forces [20], [21], joint moments [22], joint compressive forces [23], [24], joint stiffness [25], [26], and joint angles [27], [28]. The prediction performance of HNM is directly limited by the accuracy of physiological variables such as, muscle FL, PA, etc. One way to approximately model these parameters is based on simulation like OpenSim software [29]. However, parameters from simulation can hardly reflect real neuromuscular conditions. Thus, a more reliable and transparent methodology to measure subject-specific muscle structural parameters is proposed using US imaging. In [30], the authors developed a US-based approach to indirectly approximate the in vivo forces generated by human triceps surae muscles during dynamic movement tasks. In [31], they proposed the modified HNM with two contractile elements that accounted for the independent slow and fast muscle fiber contraction. This HNM was driven by US-based measures of FL, fascicle velocity, and PA. In our previous work [32], sEMG and PA from US images were combined as inputs to the HNM. The experimental results showed better dorsiflexion moment prediction performance by using the synthesized muscle activation that combines PA and sEMG than using sole PA or sEMG.

Among these studies that used neuromuscular variables to detect human motion intent, few contributions have determined a preferable muscle variable and joint moment prediction approach. The paper aims to determine the best neuromuscular signal(s) that can be used to predict ankle dorsiflexion moment generated by tibialis anterior (TA) muscle. These signals include sEMG and three signals derived from US imaging: FL, PA, and echogenicity. Muscle FL and PA are automatically extracted from US images by applying an algorithm given in [33], [34]. Furthermore, the best approach(es) among linear regression (LR), feedforward neural network (FFNN), and HNM to accurately predict the isometric ankle dorsiflexion moment are investigated.

II. METHODS

Three approaches, LR, FFNN, and HNM are discussed below to predict isometric ankle dorsiflexion moment by using four neuromuscular variables, including PA, FL, echogenicity, and sEMG.

A. Linear Regression (LR)

Among the three approaches, LR is the simplest and most straightforward approach to describe the relationship between neuromuscular variables and isometric dorsiflexion moment. The exact expression can be given as

$$y^{(i)} = \beta_j x_j^{(i)} + b_j + \varepsilon_j^{(i)}, \ i = 1, 2, ..., N$$
 (1)

where $x_j^{(i)}$ (j=1,2,3,4) represents PA, echogenicity, FL, and sEMG, respectively, at the i^{th} time instant. $y^{(i)}$ is the corresponding dorsiflexion moment computed by multiplying load cell measurement F_l and fixed moment arm r_l . β_j and b_j are the regression slope and intercept for the j^{th} variable. $\varepsilon_j^{(i)}$ is the error term or disturbance term for the j^{th} variable at the i^{th} time instant. In (1), only the input variables and observations are known. The estimated output can be represented as

$$\hat{y}_{i}^{(i)} = \beta_{i}^{*} x_{i}^{(i)} + b_{i}^{*} \tag{2}$$

where β_j^* and b_j^* are optimal values that minimize the error between observation $y^{(i)}$ and estimation $\hat{y}_j^{(i)}$. β_j^* and b_j^* are determined by defining a loss function $L(\beta_j,b_j)=\sum_{i=1}^N(\hat{y}_j^{(i)}-y^{(i)})^2$. A gradient-based search is used to calculate the following equations $\frac{\partial L}{\partial \beta_j}=0$ and $\frac{\partial L}{\partial b_j}=0$. Once the newly measured neuromuscular variables are known, the moment will be predicted by substituting β_j^* and b_j^* to (2).

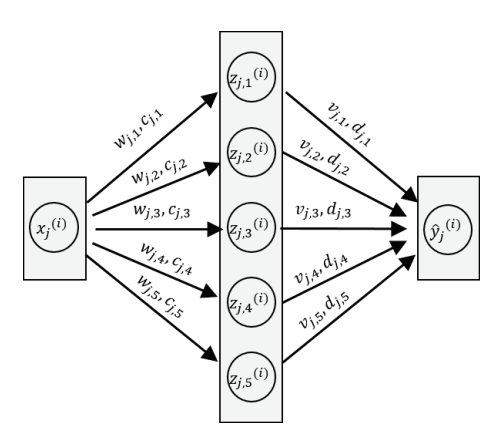


Figure 1. The structure of FFNN with a single hidden layer and 5 neurons.

B. Feedforward Neural Network (FFNN)

An FFNN is an artificial neural network where connections between the nodes do not form a cycle. In this kind of network, the information moves only in one direction; i. e., forward from the input layer to the output layer. As shown in Fig. 1, a single-layer perceptron network with five neurons was designed for data training, where the inputs are fed directly to the outputs via a series of weights and biases. Just as in LR, $x_j^{(i)}$ represent the input variables, $z_{j,p}^{(i)}$ (p=1,2,...,5) represent the states in hidden layer, and $\hat{y}_j^{(i)}$ represents the estimated output. $w_{j,p}$ and $c_{j,p}$ are the weights and biases between the input layer and hidden layer, respectively. $v_{j,p}$ and $d_{j,p}$ are the weights and biases between the hidden layer and output layer. A Sigmoid activation function $\phi(x) = \frac{1}{1+e^{-x}}$ is applied between the input layer and hidden layer. Each neuron in the hidden layer is given as

$$z_{j,p}^{(i)} = \frac{1}{1 + e^{-(w_{j,p}x_j^{(i)} + c_{j,p})}}.$$
 (3)

The estimated output is calculated as

$$\hat{y}_{j}^{(i)} = \sum_{p=1}^{5} \left(v_{j,p} z_{j,p}^{(i)} + d_{j,p} \right). \tag{4}$$

Since the dorsiflexion moment measurement is regarded as the label, the FFNN training becomes a supervised learning problem. All the weights and biases in Fig. 1 are determined by a backpropagation algorithm [35].

C. Hill-type Neuromuscular Model (HNM)

An HNM to estimate the ankle joint torque contains the following modules: neural activation, muscle activation, muscle contraction dynamics, and skeletal dynamics [36]. For the isometric ankle dorsiflexion condition, it is assumed that there is no angular position and velocity change. Therefore, the skeletal dynamics were neglected. The dorsiflexion moment generated by TA contraction equals to the multiplication of the muscle-tendon force and the corresponding constant moment arm, which is given as

$$M_{est} = F_{mt} r_{mt} \tag{5}$$

where r_{mt} is the ankle dorsiflexion moment arm represented as algebraic functions of joint angles that have been fitted to measured moment arm curves as mentioned in [37]. It is expressed as $r_{mt} = -0.013q + 0.035$ [38]. q is the angular position of ankle joint relative to the neutral position , and it is with the unit of radian. The muscle-tendon force F_{mt} generated by muscle-tendon can be expressed as

$$F_{mt} = F_m \cos(\varphi) = (F_{ce} + F_{ne}) \cos(\varphi) \tag{6}$$

where $F_{ce} = f_l(l_m)f_v(v_m)aF_{\rm max}$ denotes the force generated by the contractile element (CE), while $F_{pe} = f_p(l_m)F_{\rm max}$ denotes the force generated by the passive elastic element (PE). $F_{\rm max}$ is the TA tendon force at MVIC, which is determined by system identification, based on data collected from 3 repeated trials. l_m and v_m are the muscle FL and velocity, respectively, and φ is the pennation angle. Both l_m and φ are extracted from US images by using the commercial algorithm [33], [34], and v_m is derived by taking the time derivative of l_m . $f_l(l_m)$ and $f_v(v_m)$ represent the inherent force-fiber length relationship and force-fiber velocity relationship for the CE, respectively, and $f_p(l_m)$ represents the passive force-fiber length relationship for the PE. The explicit expressions of $f_l(l_m)$, $f_v(v_m)$, and $f_p(l_m)$ were defined in [32].

Up to this point, every term in (5) is defined, except for the muscle activation variable a. Muscle activation in HNM can be computed by using different neuromuscular variables, therefore four different muscle activation sequences $a_1^{(i)} \sim a_4^{(i)}$ are introduced here. For PA obtained from US images, the normalized values are regarded as the PA-induced muscle activation, which is defined as

$$a_1^{(i)} = \frac{x_1^{(i)} - x_{1 \min}}{x_{1 \max} - x_{1 \min}}.$$
 (7)

Similarly, for echogenicity and FL, the normalized values are regarded as the echogenicity or FL-induced muscle activation, which is defined as

$$a_m^{(i)} = \frac{x_{m \max} - x_m^{(i)}}{x_{m \max} - x_{m \min}}, m = 2, 3.$$
 (8)

The moving root mean square (MRMS) is applied to capture the characteristics of sEMG in the time domain [32], [39]. Due to the time delay between the onset of sEMG and muscle activation, a second-order recursive filter was used to calculate the neural activation $u^{(i)}$ as described in [11], which is given by considering the normalization of sEMG MRMS $N^{(i)}$

$$u^{(i)} = \alpha N^{(i-\tau)} - \delta_1 u^{(i-1)} - \delta_2 u^{(i-2)}$$
(9)

where $\alpha=0.9486$, $\delta_1=-0.056$, and $\delta_2=0.000627$. τ is the electromechanical delay (EMD), which is determined in the experimental section. As mentioned in [40], when the muscle contraction force is at a low level, there is a nonlinear relationship between neural activation and muscle activation, and beyond that level, the relationship is linear. Thus, a one-parameter segmented transfer model from neural activation $u^{(i)}$ to sEMG-induced muscle activation $a_4^{(i)}$ is designed as

$$\begin{cases} a_4^{(i)} = d \ln(cu^{(i)} + 1), \ 0 \le u^{(i)} < u_0 \\ a_4^{(i)} = mu^{(i)} + b, \ u_0 \le u^{(i)} < 1 \end{cases}$$
 (10)

The point (u_0, a_{40}) of above nonlinear model is defined as

$$\begin{cases} u_0 = 0.3085 - A\cos(\frac{\pi}{4}) \\ a_{40} = 0.3085 + A\sin(\frac{\pi}{4}) \end{cases}$$
 (11)

Knowing that the linear part of the curve in (10) must pass through both point (u_0, a_{40}) and point (1, 1), then the coefficients m and b can be determined as $m = \frac{1-a_{40}}{1-u_0}$ and $b = \frac{a_{40}-u_0}{1-u_0}$. The coefficients d and c can be determined by making the nonlinear part in (10) pass through the point (u_0, a_{40}) , then $c = \frac{e^{\frac{a_{40}}{d}}-1}{u_0}$, and d is calculated iteratively by using the Newton-Raphson method. Therefore, the four parameters d, c, m, and d are all strongly related to the point (u_0, a_{40}) , which is determined by shape coefficient d. Besides, d is reported within the range from 0 to 0.12 [40], which is to be determined by system identification.

The objective of HNM calibration procedure is to minimize the root mean square of the estimation error (RMSE) with different kinds of muscle activation by tuning the unknown parameters. The RMSE is expressed as

$$RMSE = \sqrt{\frac{1}{N} \sum_{i=1}^{N} \left(M_{est}^{(i)} - y^{(i)} \right)^{2}}.$$
 (12)

The determination of A is performed by applying MATLAB function *lqscurvefit*, and then the HNM is implemented for dorsiflexion moment prediction. New data, which is not used in the training procedure, is used for the moment prediction.

III. EXPERIMENTS

A. Participants

The study was approved by the Institutional Review Board (IRB) at the University of Pittsburgh (IRB approval number: PRO18020072). Three participants without any neuromuscular disorders were involved in this study. Participant 1: Age 25, male. Participant 2: Age 27, male. Participant 3: Age 22, male. The participants signed an informed consent form before they participated in the experiments. According to our experimental design and data processing procedures and based on the power analysis software G*Power [41], the participants would have 87% power to detect (p < 0.05) the difference between the estimated ankle dorsiflexion torques by using three approaches, with respect to the same neuromuscular signal and 92% power to detect (p < 0.05) the difference between the estimated ankle dorsiflexion torques by using four neuromuscular signals, with respect to the same approach.

B. Experimental Apparatus and Procedure

The experimental setup for this work is illustrated in Fig. 2 (d), where the participant was seated comfortably on a chair with adjustable height. Throughout the entire experimental procedure, the participant's upper leg was kept horizontal, and the lower leg was restrained perpendicular to the upper leg. To equivalently measure the dorsiflexion moment, a load cell platform was design as shown in Fig. 2 (c), where two parallel pedals with the lower pedal is fixed on a rotary shaft. A load cell sensor (MLP-300, Transducer Techniques, CA, USA) was positioned between the upper and lower pedals.

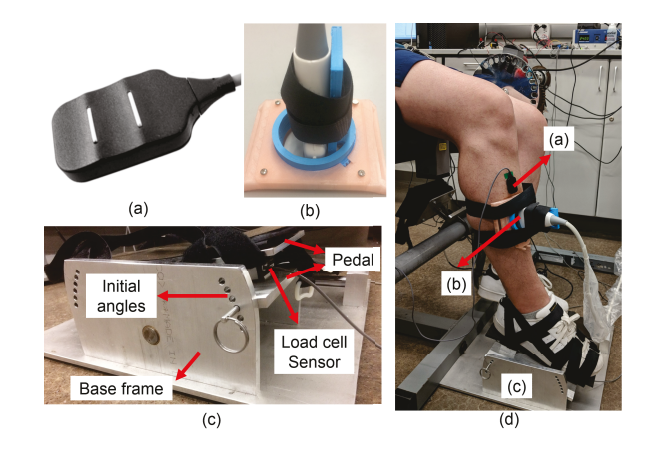


Figure 2. Experimental setup illustration. (a) Single differential sEMG sensor. (b) 3-D printed customized US probe holder with 1 degree of freedom. (c) Load cell platform with 7 adjustable angular positions. (d) Participant's initial position with sEMG sensor and US transducer attached to the targeted skin region, also with load cell pedal tied on foot.

The load cell was calibrated before each experimental session. The initial angular position of the pedals could be set as -15° , -10° , -5° , 0° , 5° , 10° , and 15° relative to the ground, which correspond to the ankle dorsiflexion angular position q in (5). So, there are 7 different experimental scenarios for each participant. The negative angle means that the perpendicular distance between toe and ground is higher than that between heel and ground. Both the toe and heel of the right foot were tied on the upper pedal of the load cell platform by using velcro straps to guarantee the isometric dorsiflexion. The equivalent moment generated by voluntary muscle contraction (VC) is computed by multiplying the load cell measurement and a constant moment arm.

The targeted region of TA was chosen as around 10 cm away from the rotation center of the knee joint on the front shank. In this targeted region, an sEMG sensor in Fig. 2 (a) (BagnoliTM Desktop, DELSYS, MA, USA) was attached to the lower leg skin through a piece of adhesive interface after the shaving and cleaning with alcohol. In the same region, a clinical linear US transducer (L7.5SC Prodigy Probe, S-Sharp, Taiwan) held by a specially customized holder (as shown in Fig. 2 (b)) was attached on the skin, and conductive US gel was applied between the transducer and participants skin. The placement of US transducer on the skin could be rotated from cross-sectional direction to longitudinal direction by the holder, and in this study, the longitudinal direction was used to achieve maximum visualization of the targeted muscle region.

The 7 scenarios were conducted in the following sequence: 0°, 5°, 10°, 15°, -5°, -10°, and -15°. Under each scenario, there were two sets of experiments. The first set was used to determine the dorsiflexion torque, TA muscle contraction force, and corresponding neuromuscular signals at MVIC. The participants were asked to perform ankle dorsiflexion by loading the load cell platform to the strongest contraction point and then unloading to a relaxed state. Each participant was verbally encouraged to elicit a maximum muscle contraction. The participants performed three repeated loading and unloading trials, where each trial lasted for 2 seconds. Three

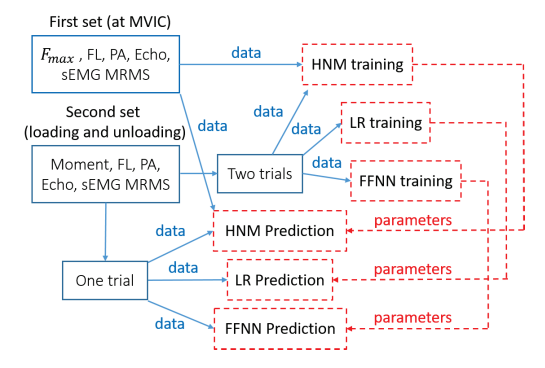


Figure 3. Flow diagram for model training and prediction.

repeated trials were performed under each scenario. At least 30 seconds of rest period was provided between two successive trials. During this experimental set, sEMG signal, load cell signal, and US imaging were recorded synchronously. In the second set experiments, there were three repeated trials, each lasting 6.12 seconds. Measurements from load cell and sEMG were collected throughout the entire duration. The 1^{st} second of each trial was left intentionally blank to initialize the US machine to get ready for imaging the TA muscle. This also allows synchronization of US imaging, sEMG, and load cell data. For the synchronization at t=2 seconds, the US machine was externally triggered by a signal sent from a real-time system designed in Matlab/Simulink (R2012b, MathWorks, MA, USA). After the trigger, the participants were verbally instructed to perform the dorsiflexion against the load cell platform. They were instructed to ramp the dorsiflexion force from zero contraction to the strongest contraction, within 1 second, and stay at the strongest contraction for around 3 seconds, before resting the muscle. All data collection was stopped at 6.12 seconds, which means that the US imaging RF data collection period was 5.12 seconds. To avoid muscle fatigue, the participants rested for 2 minutes to 4 minutes between two successive trials. Data from randomly selected two trials were used for model training and a third trial data was used for predicting the ankle dorsiflexion moment from the trained models. The flow chart of data collection, processing, training, and prediction procedures is illustrated in Fig. 3, which is detailed in the following sections.

C. Data Acquisition and Pre-processing

The measurement from the load cell was processed through an input signal conditioner (DRC-4710, OMEGA Engineering, CT, USA). In order to measure the dorsiflexion moment, the load cell measurement was multiplied by the moment arm of the testbed (0.1 m). The measurement from the sEMG sensor was processed through an input module (BagnoliTM Desktop, DELSYS, MA, USA) and a main amplifier (BagnoliTM Desktop, DELSYS, MA, USA) with an amplified gain 10k. Additionally, through this amplifier, the sEMG signal was filtered to bandwidth between 20 Hz and 450 Hz. Signals from both the conditioner and amplifier were collected by a data acquisition board (QPIDe Board, Quanser, Canada) through two analog input channels. To image the TA contraction, a

commercial linear array transducer (L7.5SC, 6.4 MHz center frequency) was used with the connection to an US scanner (Prodigy, S-Sharp, Taiwan).

A real-time system in Matlab/Simulink (R2012b, Math-Works, MA, USA) was set up to synchronize the collection of signals from the load cell and sEMG sensor at 1000 Hz. The pulse sequence (PS) mode of US imaging was applied. To guarantee the simultaneous firing time for US imaging with the real-time system in Simulink, a 1000 Hz trigger sequence with 5 % duty cycle was sent to the US scanner.

According to [42], the most commonly used time domain (TD) sEMG features include mean absolute value, zero crossings, slope sign changes, and waveform length. In addition, pre-mentioned MRMS is also a typical sEMG TD feature, which can be calculated by the following equation

$$x_4^{(i)} = \begin{cases} \left(\frac{1}{N_0} \sum_{n=i-N_0+1}^{n=i} (l^{(n)})^2\right)^{1/2}, & i \ge N_0 \\ \left(\frac{1}{i} \sum_{n=1}^{n=i} (l^{(n)})^2\right)^{1/2}, & i < N_0 \end{cases}$$
(13)

where N_0 represents the length of the moving window. For convenience, it was set as 200 ms. $l^{(n)}$ represents the amplitude of sEMG signal at each sampling instant. Under the situation with the same window length, correlation analysis between each of the sEMG features and ankle dorsiflexion moment was performed. Then MRMS was chosen to derive the neural activation in (9) due to its highest correlation coefficient with dorsiflexion torque. The results of the correlation analysis are provided in the supplementary file.

The original PS mode US imaging RF data was preprocessed through beamforming in MATLAB, and the voltage signal from the US scanner was transferred to grayscaled US images, as shown in Fig. 4. The targeted muscle during ankle dorsiflexion was the TA, which is the superficial muscle, shown in Fig. 4. The region of interest (ROI) was defined within the red dashed rectangle. For each image frame, PA was defined as the angle between the visualized fascicle and the deep aponeurosis. The orientation of the muscle fascicle and deep aponeurosis, as well as the length of the muscle fascicle $x_3^{(i)}$, were tracked frame by frame in a time sequence.

Unlike the architectural variables like PA and FL, echogenicity is a physical property of US waves when they interact with tissues. Brightness and darkness depends on how much of the US waves penetrate the tissue or are reflected back, as shown in Fig. 4, and these represent the echo bounce ability of the tissue. Higher brightness means the echo bounce is higher, which is called hyperechogenic while the darkness is called hypoechogenic. In the ROI of each frame, the grayscaled value of every pixel was computed and then the average was computed for all pixels to determine the echogenicity of the current frame $x_2^{(i)}$.

A 4^{th} -order Butterworth lowpass filter was applied for $x_j^{(i)}$ (j=1,2,3,4) to eliminate noise at high frequency. Thereafter, $x_j^{(i)}$ (j=1,2,3,4) was directly substituted in (2) of LR method and (3) of FFNN method, respectively, while the normalization (7) and (8) were regarded as muscle activation of HNM, and the normalization $N^{(i)} = \frac{x_4^{(i)} - x_4 \min}{x_4 \max - x_4 \min}$ was substituted in (9) of HNM.

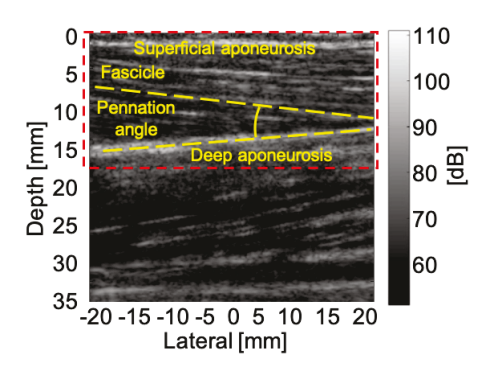


Figure 4. A typical US image of the TA. x-axis is the distance along the probe longitudinal direction, and y-axis is the depth of muscle. The RGB data of every pixel were transferred to grayscale values between 0 and 255.

D. Data Training, Prediction, and Statistical Analysis

The outcomes from data acquisition and pre-processing subsection included sEMG MRMS, PA, FL, and echogenicity. As mentioned in the previous subsection, due to a short time duration for the strongest ankle dorsiflexion and a enough resting period between two successive trials in both experimental sets, it was assumed that there was no muscle fatigue during both sets. LR and FFNN models were trained directly from the randomly selected two trials of the second experimental set. The slope and y-axis intercept of LR, and the weight matrices of FFNN were determined. Then each neuromuscular signal sequence from the third remaining trial was used as the input for the trained LR and FFNN models to predict ankle dorsiflexion moment. To train the HNM, first F_{max} , A, and the neuromuscular signals at MVIC were determined from the first experimental set. Afterwards, the HNM was trained from the randomly selected two trials in second experimental set. Finally, each neuromuscular signal sequence from the third trial was used as the input to the trained HNM model to predict ankle dorsiflexion moment.

One-way repeated-measure analysis of variance (ANOVA) followed by a Tukey's honestly significant difference test (Tukey's HSD) was applied to evaluate the training and prediction performance across four different neuromuscular signals with respect to the same mathematical model and across three different mathematical models by using the same neuromuscular signal. The significant difference level was chosen as p < 0.05.

IV. RESULTS AND DISCUSSIONS

The results are divided into three subsections: results of the first set experiments that find MVIC of the TA muscle, results of model training, and results of model prediction in the second set experiments. To simplify notation for different scenarios and different participants in the following section, the abbreviations such as, A1S0, A2S10, and A3S-10, are respectively used for the ankle angle scenarios of 0°, 10°, and -10° on the first, second, and third participant, respectively.

A. Results of MVIC

The purpose of the first set of experiments was to determine the dorsiflexion moment and the corresponding neuromuscular variables at MVIC, which were used to determine certain parameters in the HNM method. The verbal encouragement enabled the participants to generate voluntary dorsiflexion moment as strong as possible, thus there was a sub-maximal dorsiflexion moment in each trial per scenario. The 3 submaximal dorsiflexion moment values from the 3 repeated trials under each scenario are listed in Table I. The maximum and averaged values of the 3 sub-maximal values are plotted in Fig. 5. MVIC is determined as the higher dorsiflexion moment between the two highest sub-maximal values, once the difference between them is within 5 %. If the difference condition is not satisfied, the procedures were repeated until the difference condition is satisfied. Therefore, only one MVIC value exists per scenario, which is also listed in Table I. Take A1 as an example, the results show that once the pedal of the load cell platform negatively passes the neutral position, on average, the capability of generating maximum dorsiflexion moment of A01 decreases by 18.20 % (p < 0.001), 23.27 % (p < 0.001), and 30.38 % (p < 0.001) for S-5, S-10, and S-15, respectively. However, when the pedal positively passed the neutral position, this capability was increased, only within a small range, by 5.02 % (p = 0.497), 4.49 % (p = 0.614), and 2.68 % (p = 0.939) for S5, S10, and S15, respectively.

The findings in this section indicate that MVIC is related to the ankle's angular position. Considering the correlation between TA muscle length and the designed 7 scenarios, it is not hard to conclude that MVIC could have increased during TA muscle lengthening and reduced during TA muscle shortening. This effect is also known as force-enhancement and force-depression [43]. Apart from muscle length, there are many other factors that can influence MVIC in skeletal muscles. According to [44], the MVIC of the elbow flexors can be increased by local cues such as firing a gun before maximal efforts. Also, hypnosis, epinephrine injection or ingestion of amphetamine can also alter MVIC. Gandevia [45] reported a systematic review on how peripheral and central components of muscle fatigue affected voluntary muscle contraction strength. Even under conditions designed to maximize supraspinal drive, voluntary activation of muscle is commonly not maximal in measurements of isometric strength. This deficiency varies with the subject, task, time, and the muscle group [45]. Future work is needed to extract the spinal or supraspinal changes that cause the MVIC changes and to correlate those central changes with indices of performance in different participant groups and experimental tasks.

B. Results of Model Training

In the second set of experiments, the dorsiflexion moment, pre-processed sEMG, and US image variables including PA, echogenicity, and FL of the 1^{st} trial under A1S0 are shown in Fig. 6. There exists a positive correlation between PA and the moment, as well as sEMG MRMS and the moment, while a negative correlation between echogenicity and the moment, as well as FL and the moment. Although the participant

Table I
SUB-MAXIMAL DORSIFLEXION MOMENT IN EACH TRIAL AND THE DETERMINED MVIC UNDER EACH SCENARIO ON EVERY PARTICIPANT.

Scenario	A1 $(N \cdot m)$			A2 $(N \cdot m)$			A3 $(N \cdot m)$					
	Trial 1	Trial 2	Trial 3	MVIC	Trial 1	Trial 2	Trial 3	MVIC	Trial 1	Trial 2	Trial 3	MVIC
-15°	20.648	20.374	19.415	20.648	12.991	13.235	13.181	13.235	12.263	13.098	13.692	13.692
-10°	20.322	23.433	22.854	23.433	13.446	13.145	13.720	13.720	13.118	13.290	13.648	13.648
-5°	23.989	23.389	23.631	23.989	14.130	13.512	14.252	14.252	14.750	15.262	15.463	15.463
0°	28.857	27.941	30.213	30.213	15.571	16.378	16.576	16.576	18.775	16.736	17.922	18.775
5°	30.913	30.333	29.919	30.913	15.855	15.886	16.071	16.071	17.492	16.925	17.164	17.492
10°	30.369	29.743	30.595	30.595	15.505	15.655	16.472	16.472	17.570	17.125	18.273	18.273
15°	30.515	28.644	29.978	30.515	15.868	15.972	16.869	16.869	17.692	18.096	17.663	18.096

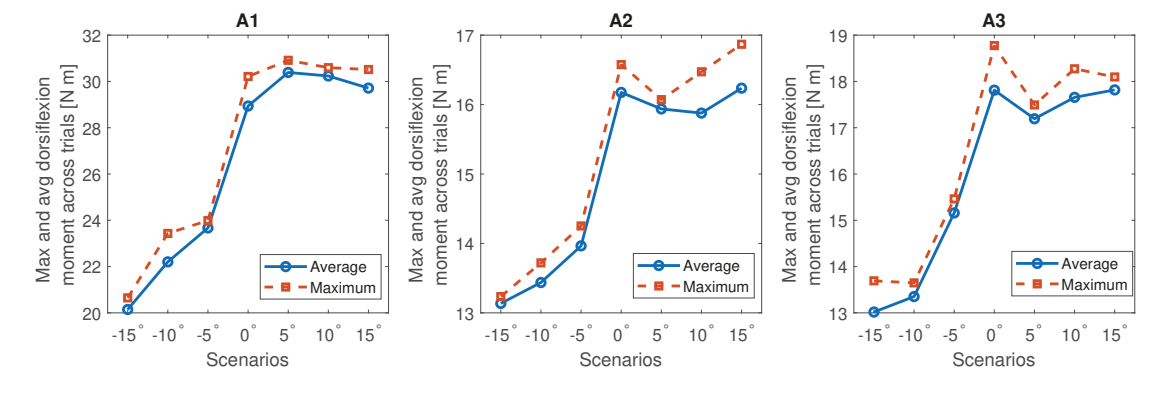


Figure 5. Maximum (MVIC) and averaged values of sub-maximal dorsiflexion moment across three trials under 7 scenarios of each participant.

was instructed verbally to maintain the maximum voluntary contraction, the generated dorsiflexion moment was prone to a decrease, as shown in Fig. 6. Similar patterns were also found in PA, FL, and sEMG MRMS. In addition, when TA recovered to a relaxed state, PA, FL, and sEMG MRMS approximately returned to the initial values, but not for echogenicity. The values of echogenicity represent the averaged grayscale value for each pixel in the ROI, and there is a time-dependent drift in the changing pattern of echogenicity. This drift implies that there exists deformation for muscle tissue after MVIC although there is no muscle contraction, and muscle tissue would not recover to initial state instantaneously. Among the four pre-processed variables, the noise in sEMG MRMS outplays than the other variables.

The EMD in (9) was defined as the delay between the onset of sEMG signal and dorsiflexion moment. To determine the EMD on each participant, the time delay values from the two training trials under each scenario were calculated and the averaged values were regarded as the EMDs, which are listed in Table II. The averaged EMDs were rounded to integer values and utilized in the HNM for both training section and prediction section due to the sampling frequency being at 1000 Hz. Due to the testing at different ankle angles, i.e., the change from -15° to 15°, the ankle angle varies from dorsiflexion to plantar flexion, which implies that the TA muscle performs eccentric contraction along this angle change sequence. For each participant, the EMD values exhibit a decreasing trend as the TA muscle length increases. These EMD results show consistency with the experimental and simulation findings in [46], [47].

The measured and estimated dorsiflexion moments from training procedure under A1S15 are shown in Fig. 7. At the

Table II EMD VALUES OF EACH PARTICIPANT IN EACH SCENARIO

Participant			E	MD (m	s)		
1 articipant	-15°	-10°	-5°	0°	5°	10°	15°
A1	64.5	53.5	49	43.5	39	35.5	29
A2	54.5	46.5	37	31	26.5	20.5	18
A3	57	51.5	45.5	38.5	33	29.5	24.5

starting of the 1st trial, the PA decreases, as seen in Fig. 6. As shown in Fig. 7 (a), the training results by using LR and HNM approaches were affected by the decreased PA value around 1.5 s; however, the FFNN approach overcame the decrease in PA. Also, as shown in Fig. 7 (d), FFNN resisted the noise in sEMG MRMS better than LR or HNM. These results indicate higher robustness of FFNN than LR or HNM. Due to the time-dependent drift of echogenicity, at some time instances, the trained data in Fig. 7 (b) did not track the measured moment well, especially for the peak values. To quantitatively evaluate the training results of each neuromuscular variable and their corresponding modeling approaches, the averaged RMSE values across scenarios between the measured and trained ankle dorsiflexion moments are listed in Table III.

C. Results of Model Prediction

Figure 8 shows the measured dorsiflexion moment and the predicted moment with respect to PA, echogenicity, FL, and sEMG under A3S15. Under this particular scenario, the results in Fig. 8 show that the prediction with respect to echogenicity exhibits the worst performance, while the results with respect to PA and FL exhibit much better prediction. In addition, results in Fig. 8 (d) indicate the FFNN approach is more robust to sEMG signal noise, compared to LR and HNM approaches.

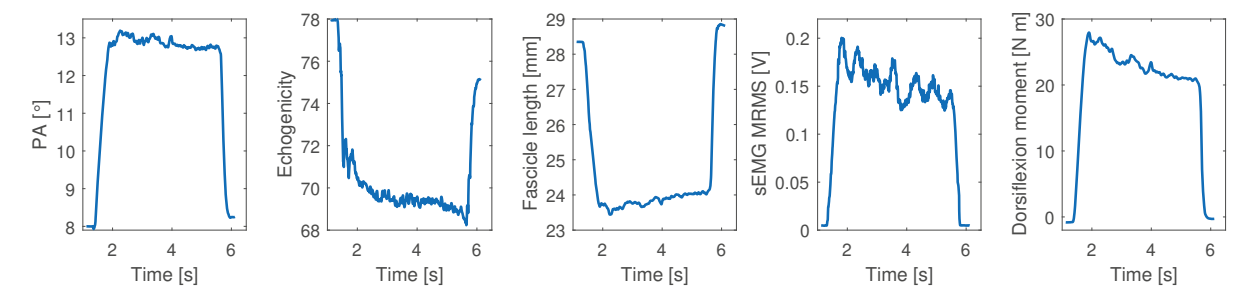


Figure 6. Variables measured using US images, sEMG MRMS, and the corresponding dorsiflexion moment during 1st trial under A1S0.

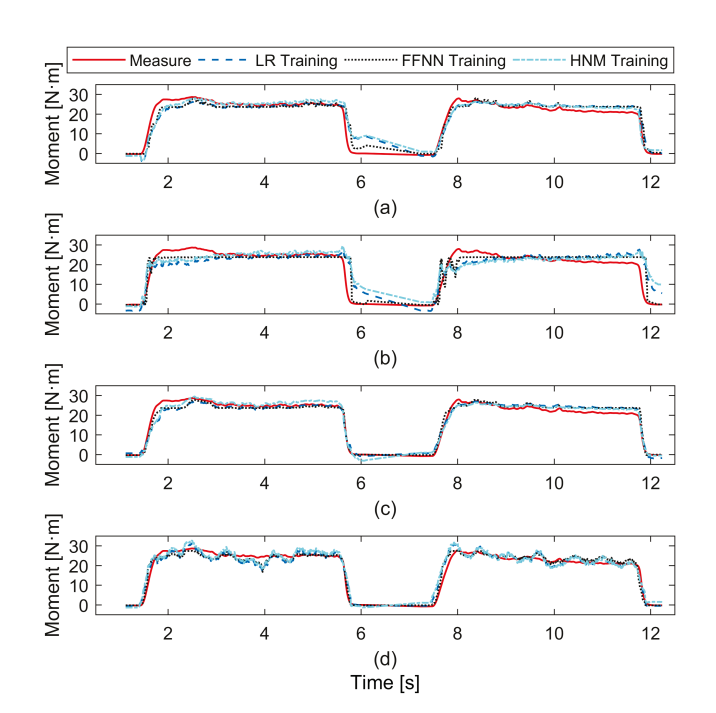


Figure 7. Ankle dorsiflexion moments from training and measurement under A1S15. (a) Training with PA. (b) Training with echogenicity. (c) Training with FL. (d) Training with MRMS of sEMG.

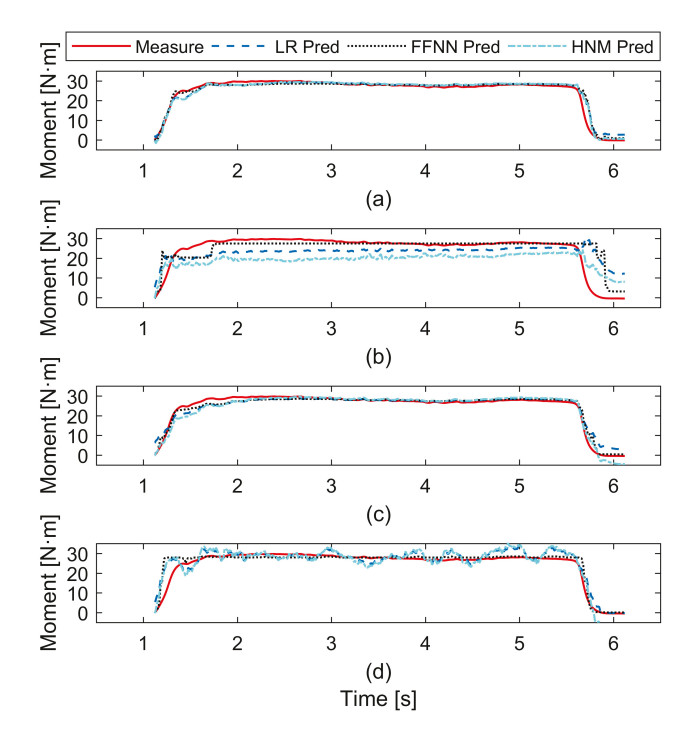


Figure 8. Ankle dorsiflexion moment from prediction and measurement under A3S15. (a) Prediction with PA. (b) Prediction with echogenicity. (c) Prediction with FL. (d) Prediction with MRMS of sEMG.

Table III
RMSE values (average±standard deviation) across scenarios
BETWEEN TRAINED AND MEASURED DORSIFLEXION MOMENTS FOR EACH
PARTICIPANT

		RMSE $(N \cdot m)$					
Variable	Method	A1	A2	A3			
	LR	2.217 (0.673)	2.483 (1.274)	2.104 (0.572)			
PA	FFNN	1.831 (0.640)	2.053 (1.354)	1.411 (0.568)			
	HNM	1.688 (0.744)	1.712 (0.534)	1.953 (0.513)			
	LR	5.176 (0.431)	3.598 (1.444)	2.444 (0.884)			
Echo	FFNN	4.033 (0.613)	2.520 (0.970)	1.926 (0.864)			
	HNM	3.540 (0.551)	2.222 (1.014)	2.666 (1.105)			
	LR	2.308 (0.743)	3.039 (1.069)	1.341 (0.708)			
FL	FFNN	1.626 (0.527)	2.134 (1.112)	0.773 (0.520)			
	HNM	1.284 (0.230)	2.814 (1.183)	1.174 (0.744)			
	LR	3.341 (0.871)	2.241 (0.310)	2.212 (0.320)			
sEMG	FFNN	2.280 (0.657)	1.909 (0.211)	1.692 (0.398)			
	HNM	3.228 (1.266)	2.306 (0.186)	2.810 (0.631)			

The averaged RMSE values and standard deviations between the measured (actual) and predicted dorsiflexion moments across all scenarios were computed to obtain a quantitative evaluation of the prediction algorithms, when different approaches and neuromuscular variables were used. These results are listed in Table IV. The results show that for the same approach, RMSE value of the echogenicity-based prediction across all scenarios is higher than the RMSE values of the PA, FL, or sEMG-based prediction. Meanwhile, for each neuromuscular variable, the RMSE values of both FFNN and HNM were lower than the LR modeling approach.

To determine if the findings can be generalized for an individual, validation across scenarios and participants (VASP) was performed on the data collected from all three participants. The results in Fig. 9 show that when PA is used as a neuromuscular variable, the RMSE values of FFNN and HNM are lower than the RMSE values of LR by 19.64 % (p=0.323) and 27.26 % (p=0.119), respectively. When echogenicity is

Table IV

RMSE VALUES (AVERAGE±STANDARD DEVIATION) ACROSS SCENARIOS
BETWEEN PREDICTED AND MEASURED DORSIFLEXION MOMENTS FOR
EACH PARTICIPANT

	Method	RMSE $(N \cdot m)$					
variable		A1	A2	A3			
	LR	2.683 (1.294)	3.653 (1.232)	2.711 (0.933)			
PA	FFNN	1.998 (0.657)	3.111 (1.660)	2.038 (0.701)			
	HNM	2.111 (0.517)	2.639 (1.449)	1.712 (0.549)			
	LR	5.730 (1.499)	3.942 (1.388)	2.978 (1.425)			
Echo	FFNN	4.962 (1.064)	3.365 (1.656)	2.588 (1.449)			
	HNM	4.518 (0.835)	3.233 (1.530)	3.116 (2.149)			
	LR	2.603 (1.551)	3.171 (0.882)	1.635 (0.568)			
FL	FFNN	2.138 (1.446)	2.131 (1.279)	1.263 (0.358)			
	HNM	2.452 (1.417)	2.662 (1.220)	1.042 (0.539)			
-	LR	2.969 (0.942)	2.267 (0.509)	1.901 (0.184)			
sEMG	FFNN	1.970 (0.694)	2.147 (0.438)	1.729 (0.645)			
	HNM	2.665 (0.903)	2.312 (0.346)	1.834 (0.323)			

used as a neuromuscular variable, the RMSE values of FFNN and HNM are lower than the RMSE values of LR by 11.85 % (p=0.653) and 9.58 % (p=0.756), respectively. When FL is used as a neuromuscular variable, the RMSE values of FFNN and HNM are lower than the RMSE values of LR by 2.50 % (p=0.995) and 13.93 % (p=0.844), respectively. When sEMG is used as a neuromuscular variable, the RMSE values of FFNN and HNM are lower than the RMSE values of LR by 20.26 % (p=0.079) and 5.20 % (p=0.838), respectively. However, as can be seen by the p-values, no statistical significant difference was found among different approaches with respect to the same neuromuscular variable.

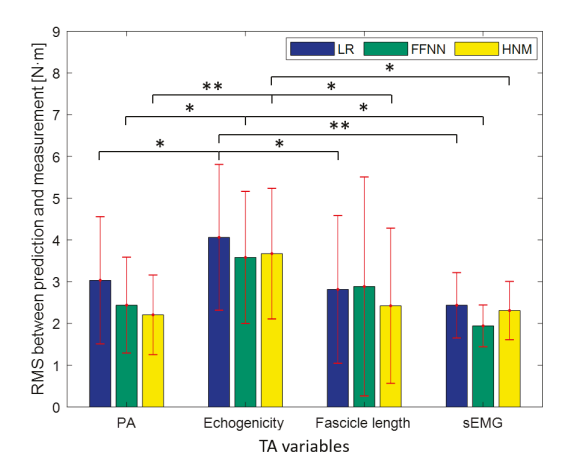
The results in Fig. 9 also show that in the LR approach, when PA, FL, and sEMG are used, the RMSE values are significantly lower than the RMSE values, when echogenicity is used, by 28.32 % (p < 0.05), 30.70 % (p < 0.05), and 40.05 % (p < 0.01), respectively. In the FFNN approach, when PA, FL, and sEMG are used, the RMSE values are significantly lower than the RMSE values, when echogenicity is used, by 31.92 % (p < 0.05), 19.43 % (p = 0.491), and 45.78 % (p < 0.05), respectively. In the HNM approach, when PA, FL, and sEMG are used, the RMSE values are significantly lower than the RMSE values, when echogenicity is used, by 39.92 % (p < 0.01), 34.04 % (p < 0.05), and 37.15 % (p < 0.05), respectively. The results of R^2 values show that in the LR approach, when PA, FL, and sEMG are used, the R^2 values are significantly increased than the R^2 values, when echogenicity is used, by 19.32 % (p < 0.01), 16.73 % (p < 0.05), and 18.35 % (p < 0.05), respectively. In the FFNN approach, when PA, FL, and sEMG are used, the R^2 values are significantly increased than the R^2 values, when echogenicity is used, by 16.17 % (p = 0.207), 4.21 % (p = 0.955), and 19.93 % (p < 0.05), respectively. In the HNM approach, when PA, FL, and sEMG are used, the R^2 values are significantly increased than the R^2 values, when echogenicity is used, by 16.81 % (p < 0.05), 12.73 % (p =0.138), and 12.79 % (p = 0.135), respectively. However, there is no significant difference of the RMSE error or R^2 values among LR, FFNN, and HNM approaches with respect to each of the neuromuscular variable.

D. Discussions

In this paper, voluntary ankle dorsiflexion effort was detected and evaluated by using Hill-type neuromuscular modelbased and model-free approaches. The sEMG MRMS and US imaging-derived signals, PA, FL, and echogenicity, were evaluated as non-invasive neuromuscular signals to predict the voluntary ankle effort. There are three reasons for selecting PA, FL, and echogenicity as the features from US images. The first one is that, in existing literature, the three features are the most frequently used US image features for voluntary effort prediction [48]–[51]. These features have high correlation with muscle or joint mechanical functions as described in the introduction section. The second reason is that these three features represent morphological information (PA and FL) and functional information (echogenicity). We want to investigate if either of these two information could be used as an indicator for muscle activation level. The third reason is that a HNM is used to predict ankle dorsiflexion moment, where PA and FL are used to represent muscular geometry in the HNM model. Echogenicity is an easily accessible measurement derived from ultrasound imaging that does not require complex tracking algorithms; thus, saving processing time and potentially enabling real-time implementation with minimal efforts in the future.

The comparisons among different mathematical approaches with respect to the same neuromuscular variable, and among different neuromuscular variables corresponding to the same mathematical approach were performed. Moreover, this is the first study investigating both model-free and model-based approaches for detecting human ankle dorsiflexion intent by using multiple non-invasive neuromuscular variables. The results in Table IV are consistent with the results in [50], where the PCC between MVIC and muscle thickness, PA, and echogenicity were compared. Both muscle thickness and PA showed higher PCC with MVIC than echogenicity in both young and elderly groups. Furthermore, multiple regression analysis revealed that muscle thickness had the best correlation with MVIC. Similarly, in [52], the results suggested that echo intensity (EI) obtained from the quadriceps femoris muscle was related to the muscular power and functional capacity of older subjects. However, it was shown that the EI in some regions of the quadriceps muscle may not correlate well with muscular performance. The possible reason is that the echogenicity variable is sensitive to the orientation of the US probe, the relative movement between the US probe and the skin, as well as the pressure on the skin.

In terms of the robustness for the 3 mathematical approaches, as shown in Fig. 7 and Fig. 8, when the sEMG signal was used as a neuromuscular variable, FFNN had the highest robustness to the inherent noise in the signal, compared to the LR and HNM approaches. A possible reason is that the nonlinear multiple-layer NN and backpropagation algorithm can be trained to act as a digital filter that minimizes the noise effects. For model-free methodology, just like the LR and FFNN approaches used in this paper, in [49] nonlinear regression like exponential function was utilized to determine the relationship between each US parameter and EMG. In [13] polynomial



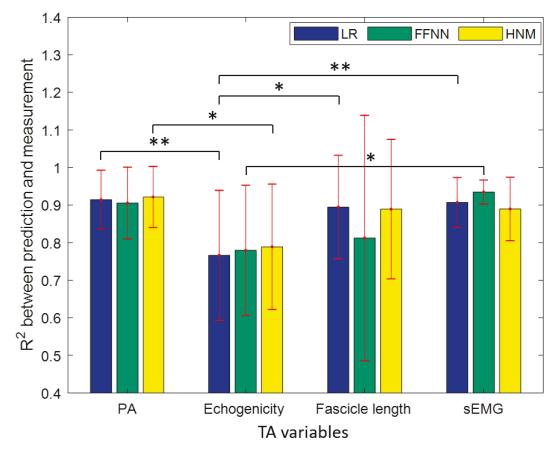


Figure 9. Average values and standard deviation of RMSE and R^2 between measured and predicted dorsiflexion moments in VASP. *, **, and *** represent the significant difference level at p < 0.05, p < 0.01, and p < 0.001.

regression analyses were performed to correlate isometric leg extension torque with US imaging-derived cross-sectional area and width-thickness ratio, EMG RMS, and mechanomyography RMS. However, the frame rate of B-mode US imaging was 25 Hz, which was much lower than 1000 Hz used in this paper. Furthermore, the isometric torque estimation or prediction performance was not validated in a continuous timedomain. Thus, the estimation or prediction method may not be practical as a real-time feedback in neurorehabilitation device control. For model-based methodology, in [53], the parameters of HNM including the shape coefficient, maximum muscle contraction force, and tendon slack length were calibrated, while other neuromuscular parameters including PA, FL, and tendon length were assigned using the simulation software OpenSim. This approximation approach essentially neglected subjective differences in PA and FL among participants. This issue is addressed in this study by including person-specific variables: PA, FL, and echogenicity that were extracted from real-time US images. In [31], the authors also considered sEMG signal and US imaging-derived variables to implement an HNM approach that used a differential model with two contractile elements to account for both slow and fast contraction fibers. In the aforementioned contributions, the muscle activation in HNM was only based on the transformation from neural activation, which was only related to the normalization of pre-processed sEMG signal. In our study, except for sEMGinduced muscle activation, US image variable-induced muscle activation was also utilized in the HNM approach, which means that the subject-specific measures from US images were not only used for muscle contraction model but also used for muscle activation model.

Although sEMG, US imaging, and load cell signals were recorded at 1000 Hz in real-time, the processing and analysis were done off-line. The targeted muscle fascicles from US images had to be initially defined in the first frame of the image sequence, before the algorithm *Muscle Fascicle Tracking* could be used. Additionally, the fascicle tracking algorithm is dependent on US images with visually distinct fascicles and aponeurosis, which may not be practical when fascicles

cannot be distinguished with US images such as in multipennate muscles. To realize real-time operation, an extensive investigation and engineering efforts are required. Therefore, real-time implementation was not included in the current work of which the main focus is to report the evaluation of isometric ankle dorsiflexion moment prediction by using various neuromuscular signals, as well as neuromuscular model-based and model-free approaches. Further work should involve two aspects: 1) sEMG and US imaging features extraction in real-time and 2) ankle dorsiflexion moment prediction in real-time. While for sEMG feature extraction, there is no doubt that sEMG MRMS can be obtained in real-time at 1000 Hz, for US imaging features extraction, we suggest the use of parallel computing framework on a graphical processing unit to improve image processing time [54].

The results in this work focus on people without neurological disorders. The architectural features and echogenicity derived from US images of pathological skeletal muscles may differ from those of normal muscles. As studied in [55], the authors revealed the fundamental differences in architectural and mechanical properties of the ankle joint and medial gastrocnemius muscle fascicles between young adults with spastic cerebral palsy and typically developed age-matched controls. In [56], the authors found a markedly varied muscle deformation pattern between patients group with facioscapulohumeral muscular dystrophy and healthy patients group, where patients with severe peroneal weakness showed less displacement of the central tendon region of TA muscle, while the healthy patients showed a non-uniform displacement pattern with the central aponeurosis showing the largest displacement. For the muscles with pathological change, there might be performance degradation of the proposed methods, but it is hard to determine until investigation is performed. Therefore, for the proposed methods to find its application in assistive devices control, further investigation on impaired muscles will be needed in our future work.

During the experiments, we ensured that all devices were stable on the targeted skin position, especially the ultrasound transducer. However, a limitation of the study is that the robustness of the prediction performance to slippage or to the effects of different attachment points after removing the sensors remains to be studied. Secondly, although HNM was widely used for joints mechanical functions detection, like muscle contraction force, joint moment, joint angle, and joint stiffness, one general, and so far neglected problem in the presented HNM approach is that it fails to reproduce muscle force or joint moment in dynamic contractions, where the muscle length is joint angle-dependent. As mentioned in [43], muscle force increases during and after active muscle lengthening (known as Force-enhancement), and reduces during and after active muscle shortening (known as Force-depression). During the dynamic contractions, the effects of muscle contraction history may have a crucial role for muscle force or joint moment prediction, which are not addressed in the presented HNM approach. Due to compliance of series elastic structures, even during quasi isometric (end held) contractions, there is a substantial shortening of the muscle fascicle (shown in Fig. 6). Thus, prediction of realistic muscle forces (and joint moments) based on sEMG and US imaging data requires consideration of contraction history effects in the muscle models. Especially, extension of the scope of the method to nonisometric contractions (e.g. every day movements including muscle-tendon complex shortening and lengthening) requires consideration of contraction history effects. There exist a series of further developments in muscle models [57]-[59] that enable the reproduction of Force-enhancement and Forcedepression during dynamic muscle contraction. The models that consider these enhancements will be investigated in our future work. Furthermore, the current study assumed that there was no angular position and velocity change in the isometric ankle dorsiflexion situation, because two effective ways were designed in the experiments: 1) participants were asked to wear hard and tight shoes, 2) both toe and heel were tied on the upper pedal of the load cell platform tightly by using velcro straps. However, due to the soft tissue of the foot and small movements in the foot joints (e.g. tarsometatarsal joints/Lisfranc joints), movements between TA muscle and origin will be expected. The influence of those small movement on neuromuscular variables like PA and FL has not been considered in the paper, which needs to be investigated in the future experiments.

V. CONCLUSION

In this study, model-free methods, LR and FFNN, as well as a model-based method, HNM, were applied to predict voluntary human ankle dorsiflexion moment with respect to different neuromuscular variables from both US images and sEMG. Under 7 scenarios, sEMG, US imaging, and load cell signals were simultaneously recorded in real-time from the voluntary isometric dorsiflexion of three participants. The results from VASP showed that with respect to the same variable there was no significant difference among three approaches, but using the same approach, the prediction performance was significantly improved by using PA, FL, and sEMG in comparison with echogenicity, respectively. The findings in this study determined a better neuromuscular variable and better modeling

approaches for detecting human lower limb movement intent non-invasively. In the future work, validations of non-isometric ankle dorsiflexion movement are necessary to generalize the findings in this work. This is essential for a practical implementation of motorized or FES-assisted rehabilitation devices.

Acknowledgment. The authors would like to thank the reviewers for the constructive comments and suggestions, which are extremely helpful for us to improve the manuscript.

REFERENCES

- H. B. Menz, M. E. Morris, and S. R. Lord, "Foot and ankle characteristics associated with impaired balance and functional ability in older people," *J. Gerontol. A Biol. Sci. Med. Sci.*, vol. 60, no. 12, pp. 1546–1552, 2005.
- [2] D. G. Everaert, A. K. Thompson, S. L. Su Ling Chong, and R. B. Stein, "Does Functional Electrical Stimulation for Foot Drop Strengthen Corticospinal Connections?" *Neurorehabil. Neural Repair*, vol. 24, no. 2, pp. 168–177, 2010.
- [3] G. Chen, C. K. Chan, Z. Guo, and H. Yu, "A Review of Lower Extremity Assistive Robotic Exoskeletons in Rehabilitation Therapy," *Crit. Rev. Biomed. Eng.*, vol. 41, no. 4-5, pp. 343–363, 2013.
- [4] A. U. Pehlivan, D. P. Losey, and M. K. OMalley, "Minimal Assist-as-Needed Controller for Upper Limb Robotic Rehabilitation," *IEEE Trans. Robot.*, vol. 32, no. 1, pp. 113–124, 2016.
- [5] M. Shahbazi, S. F. Atashzar, M. Tavakoli, and R. V. Patel, "Robotics-Assisted Mirror Rehabilitation Therapy: A Therapist-in-the-Loop Assistas-Needed Architecture," *IEEE/ASME Trans. Mechatron.*, vol. 21, no. 4, pp. 1954–1965, 2016.
- [6] J. Lobo-Prat, P. N. Kooren, A. H. Stienen, J. L. Herder, B. F. Koopman, and P. H. Veltink, "Non-invasive control interfaces for intention detection in active movement-assistive devices," *J. Neuroeng. Rehabil.*, vol. 11, no. 1, p. 168, 2014.
- [7] J. Sun, Z. Guo, Y. Zhang, X. Xiao, and J. Tan, "A Novel Design of Serial Variable Stiffness Actuator Based on an Archimedean Spiral Relocation Mechanism," *IEEE ASME Trans. Mechatron.*, vol. 23, no. 5, pp. 2121– 2131, 2018.
- [8] Q. Zhang, D. Sun, W. Qian, X. Xiao, and Z. Guo, "Modeling and control of a cable-driven rotary series elastic actuator for an upper limb rehabilitation robot," *Front. Neurorobot.*, vol. 14, 2020.
- [9] D. Zanotto, Y. Akiyama, P. Stegall, and S. K. Agrawal, "Knee Joint Misalignment in Exoskeletons for the Lower Extremities: Effects on User's Gait," *IEEE Trans. Robot.*, vol. 31, no. 4, pp. 978–987, 2015.
- [10] R. Gopura, D. Bandara, K. Kiguchi, and G. Mann, "Developments in hardware systems of active upper-limb exoskeleton robots: A review," *Rob. Auton. Syst.*, vol. 75, pp. 203–220, 2016.
- [11] D. G. Lloyd and T. F. Besier, "An EMG-driven musculoskeletal model to estimate muscle forces and knee joint moments in vivo," *J. Biomech.*, vol. 36, no. 6, pp. 765–776, 2003.
- [12] J. Shi, Y. P. Zheng, Q. H. Huang, and X. Chen, "Continuous monitoring of sonomyography, electromyography and torque generated by normal upper arm muscles during isometric contraction: Sonomyography assessment for arm muscles," *IEEE Trans. Biomed. Eng.*, vol. 55, no. 3, pp. 1191–1198, 2008.
- [13] J.-Y. Guo, Y.-P. Zheng, H.-B. Xie, and X. Chen, "Continuous monitoring of electromyography (EMG), mechanomyography (MMG), sonomyography (SMG) and torque output during ramp and step isometric contractions," *Med. Eng. Phys.*, vol. 32, no. 9, pp. 1032–1042, 2010.
- [14] Y. Zeng, J. Yang, C. Peng, and Y. Yin, "Evolving Gaussian Process Autoregression based Learning of Human Motion Intent Using Improved Energy Kernel Method of EMG," *IEEE Trans. Biomed. Eng.*, pp. 1–10, 2019.
- [15] Q. Zhang, Z. Sheng, F. Moore-Clingenpeel, K. Kim, and N. Sharma, "Ankle dorsiflexion strength monitoring by combining sonomyography and electromyography," in *Proc. Int. Conf. Rehabil. Robot.* IEEE, 2019, pp. 240–245.
- [16] S. Sikdar, H. Rangwala, E. B. Eastlake, I. A. Hunt, A. J. Nelson, J. Devanathan, A. Shin, and J. J. Pancrazio, "Novel method for predicting dexterous individual finger movements by imaging muscle activity using a wearable ultrasonic system," *IEEE Trans. Neural Syst. Rehabil. Eng.*, vol. 22, no. 1, pp. 69–76, 2013.

- [17] A. S. Dhawan, B. Mukherjee, S. Patwardhan, N. Akhlaghi, G. Diao, G. Levay, R. Holley, W. M. Joiner, M. Harris-Love, and S. Sikdar, "Proprioceptive sonomyographic control: A novel method for intuitive and proportional control of multiple degrees-of-freedom for individuals with upper extremity limb loss," Sci. Rep., vol. 9, no. 1, pp. 1–15, 2019.
- [18] H. H. Savelberg and W. Herzog, "Prediction of dynamic tendon forces from electromyographic signals: An artificial neural network approach," *J. Neurosci. Methods*, vol. 78, no. 1-2, pp. 65–74, 1997.
- [19] H.-B. Xie, Y.-P. Zheng, J.-Y. Guo, X. Chen, and J. Shi, "Estimation of wrist angle from sonomyography using support vector machine and artificial neural network models," *Med. Eng. Phys.*, vol. 31, no. 3, pp. 384–391, 2009.
- [20] M. Sartori, M. Reggiani, E. Pagello, and D. G. Lloyd, "Modeling the Human Knee for Assistive Technologies," *IEEE Trans. Biomed. Eng.*, vol. 59, no. 9, pp. 2642–2649, 2012.
- [21] T. F. Besier, M. Fredericson, G. E. Gold, G. S. Beaupré, and S. L. Delp, "Knee muscle forces during walking and running in patellofemoral pain patients and pain-free controls," *J. Biomech.*, vol. 42, no. 7, pp. 898–905, 2009.
- [22] M. Sartori, D. Farina, and D. G. Lloyd, "Hybrid neuromusculoskeletal modeling to best track joint moments using a balance between muscle excitations derived from electromyograms and optimization," *J. Biomech.*, vol. 47, no. 15, pp. 3613–3621, 2014.
- [23] P. Gerus, M. Sartori, T. F. Besier, B. J. Fregly, S. L. Delp, S. A. Banks, M. G. Pandy, D. D. D'Lima, and D. G. Lloyd, "Subject-specific knee joint geometry improves predictions of medial tibiofemoral contact forces," *J. Biomech.*, vol. 46, no. 16, pp. 2778–2786, 2013.
- [24] J. Fernandez, M. Sartori, D. Lloyd, J. Munro, and V. Shim, "Bone remodelling in the natural acetabulum is influenced by muscle forceinduced bone stress," *Int. J. Numer. Method Biomed. Eng.*, vol. 30, no. 1, pp. 28–41, 2014.
- [25] S. Pfeifer, H. Vallery, M. Hardegger, R. Riener, and E. J. Perreault, "Model-Based Estimation of Knee Stiffness," *IEEE Trans. Biomed. Eng.*, vol. 59, no. 9, pp. 2604–2612, 2012.
- [26] M. Sartori, M. Maculan, C. Pizzolato, M. Reggiani, and D. Farina, "Modeling and simulating the neuromuscular mechanisms regulating ankle and knee joint stiffness during human locomotion," *J. Neurophysiol.*, vol. 114, no. 4, pp. 2509–2527, 2015.
- [27] J. W. Pau, S. S. Xie, and A. J. Pullan, "Neuromuscular interfacing: Establishing an emg-driven model for the human elbow joint," *IEEE Trans. Biomed. Eng.*, vol. 59, no. 9, pp. 2586–2593, 2012.
- [28] M. H. Jahanandish, N. P. Fey, and K. Hoyt, "Lower-Limb Motion Estimation Using Ultrasound Imaging: A Framework For Assistive Device Control," *IEEE J. Biomed. Health Inform.*, pp. 1–10, 2019.
- [29] S. Yao, Y. Zhuang, Z. Li, and R. Song, "Adaptive admittance control for an ankle exoskeleton using an EMG-driven musculoskeletal model," *Front. Neurorobot.*, vol. 12, 2018.
- [30] T. J. Dick, A. S. Arnold, and J. M. Wakeling, "Quantifying Achilles tendon force in vivo from ultrasound images," *J. Biomech.*, vol. 49, no. 14, pp. 3200–3207, 2016.
- [31] T. J. M. Dick, A. A. Biewener, and J. M. Wakeling, "Comparison of human gastrocnemius forces predicted by Hill-type muscle models and estimated from ultrasound images," *J. Exp. Biol.*, vol. 220, no. 9, pp. 1643–1653, 2017.
- [32] Q. Zhang, K. Kim, and N. Sharma, "Prediction of ankle dorsiflexion moment by combined ultrasound sonography and electromyography," *IEEE Trans. Neural Syst. Rehabil. Eng.*, vol. 28, no. 1, pp. 318–327, 2019.
- [33] N. J. Cronin, C. P. Carty, R. S. Barrett, and G. Lichtwark, "Automatic tracking of medial gastrocnemius fascicle length during human locomotion," *J. Appl. Biomech.*, vol. 111, no. 5, pp. 1491–1496, 2011.
- [34] J. G. Gillett, R. S. Barrett, and G. A. Lichtwark, "Reliability and accuracy of an automated tracking algorithm to measure controlled passive and active muscle fascicle length changes from ultrasound," *Comput. Methods Biomech. Biomed. Engin.*, vol. 16, no. 6, pp. 678– 687, 2013.
- [35] M. A. Nielsen, Neural networks and deep learning. Determination press San Francisco, CA, USA:, 2015, vol. 25.
- [36] E. K. Chadwick, D. Blana, R. F. Kirsch, and A. J. Van Den Bogert, "Real-time simulation of three-dimensional shoulder girdle and arm dynamics," *IEEE Trans. Biomed. Eng.*, vol. 61, no. 7, pp. 1947–1956, 2014.
- [37] C. Spoor, J. Van Leeuwen, C. Meskers, A. Titulaer, and A. Huson, "Estimation of instantaneous moment arms of lower-leg muscles," *J. Biomech.*, vol. 23, no. 12, pp. 1247–1259, 1990.

- [38] R. Riener and T. Fuhr, "Patient-driven control of FES-supported standing up: A simulation study," *IEEE Trans. Rehabil. Eng.*, vol. 6, pp. 113–124, 1998.
- [39] K. Watanabe and H. Akima, "Normalized EMG to normalized torque relationship of vastus intermedius muscle during isometric knee extension," Eur. J. Appl. Physiol., vol. 106, no. 5, pp. 665–673, 2009.
- [40] K. Manal and T. S. Buchanan, "A one-parameter neural activation to muscle activation model: estimating isometric joint moments from electromyograms," J. Biomech., vol. 36, no. 8, pp. 1197–1202, 2003.
- [41] F. Faul, E. Erdfelder, A. Buchner, and A.-G. Lang, "Statistical power analyses using g* power 3.1: Tests for correlation and regression analyses," *Behav. Res. Methods*, vol. 41, no. 4, pp. 1149–1160, 2009.
- [42] B. Hudgins, P. Parker, and R. N. Scott, "A new strategy for multifunction myoelectric control," *IEEE Trans. Biomed. Eng.*, vol. 40, no. 1, pp. 82– 94, 1993.
- [43] B. Abbott and X. Aubert, "The force exerted by active striated muscle during and after change of length," J. Physiol., vol. 117, no. 1, p. 77, 1952
- [44] M. Ikai and A. H. Steinhaus, "Some factors modifying the expression of human strength," J. Appl. Physiol., vol. 16, no. 1, pp. 157–163, 1961.
- [45] S. C. Gandevia, "Spinal and supraspinal factors in human muscle fatigue," *Physiol. Rev.*, vol. 81, no. 4, pp. 1725–1789, 2001.
- [46] F. Mörl, T. Siebert, S. Schmitt, R. Blickhan, and M. Guenther, "Electro-mechanical delay in hill-type muscle models," *J. Mech. Med. Biol.*, vol. 12, no. 05, p. 1250085, 2012.
- [47] L. Schmid, T. Klotz, T. Siebert, and O. Röhrle, "Characterization of electromechanical delay based on a biophysical multi-scale skeletal muscle model," *Front. Physiol.*, vol. 10, p. 1270, 2019.
- [48] T. Fukunaga, Y. Ichinose, M. Ito, Y. Kawakami, and S. Fukashiro, "Determination of fascicle length and pennation in a contracting human muscle in vivo," *J. Appl. Physiol.*, vol. 82, no. 1, pp. 354–358, 1997.
- [49] P. Hodges, L. Pengel, R. Herbert, and S. Gandevia, "Measurement of muscle contraction with ultrasound imaging," *Muscle & Nerve*, vol. 27, no. 6, pp. 682–692, 2003.
- [50] E. M. Strasser, T. Draskovits, M. Praschak, M. Quittan, and A. Graf, "Association between ultrasound measurements of muscle thickness, pennation angle, echogenicity and skeletal muscle strength in the elderly," Age, vol. 35, no. 6, pp. 2377–2388, 2013.
- [51] Z. A. Puthucheary, R. Phadke, J. Rawal, M. J. McPhail, P. S. Sidhu, A. Rowlerson, J. Moxham, S. Harridge, N. Hart, and H. E. Montgomery, "Qualitative ultrasound in acute critical illness muscle wasting," *Crit. Care Med.*, vol. 43, no. 8, pp. 1603–1611, 2015.
- [52] E. N. Wilhelm, A. Rech, F. Minozzo, R. Radaelli, C. E. Botton, and R. S. Pinto, "Relationship between quadriceps femoris echo intensity, muscle power, and functional capacity of older men," *Age*, vol. 36, no. 3, pp. 1113–1122, jun 2014.
- [53] D. Ao, R. Song, and J. Gao, "Movement Performance of Human-Robot Cooperation Control Based on EMG-Driven Hill-Type and Proportional Models for an Ankle Power-Assist Exoskeleton Robot," *IEEE Trans. Neural Syst. Rehabil. Eng.*, vol. 25, no. 8, pp. 1125–1134, 2017.
- [54] Z. Sheng, N. Sharma, and K. Kim, "Quantitative assessment of changes in muscle contractility due to fatigue during nmes: An ultrasound imaging approach," *IEEE Trans. Biomed. Eng.*, vol. 67, no. 3, pp. 832– 841, 2019.
- [55] L. Barber, R. Barrett, and G. Lichtwark, "Passive muscle mechanical properties of the medial gastrocnemius in young adults with spastic cerebral palsy," *J. Biomech.*, vol. 44, no. 13, pp. 2496–2500, 2011.
- [56] K. Gijsbertse, R. Goselink, S. Lassche, M. Nillesen, A. Sprengers, N. Verdonschot, N. van Alfen, and C. De Korte, "Ultrasound imaging of muscle contraction of the tibialis anterior in patients with facioscapulohumeral dystrophy," *Ultrasound Med. Biol.*, vol. 43, no. 11, pp. 2537– 2545, 2017.
- [57] O. Till, T. Siebert, C. Rode, and R. Blickhan, "Characterization of isovelocity extension of activated muscle: a hill-type model for eccentric contractions and a method for parameter determination," *J. Theor. Biol.*, vol. 255, no. 2, pp. 176–187, 2008.
- [58] C. Disselhorst-Klug, T. Schmitz-Rode, and G. Rau, "Surface electromyography and muscle force: Limits in semg-force relationship and new approaches for applications," *Clin. Biomech.*, vol. 24, no. 3, pp. 225–235, 2009.
- [59] G. Schappacher-Tilp, T. Leonard, G. Desch, and W. Herzog, "A novel three-filament model of force generation in eccentric contraction of skeletal muscles," *PloS one*, vol. 10, no. 3, 2015.